J. Fluid Mech. (1995), *vol.* 287, *pp.* 93–118

Asymptotic solution of shock tube flows with homogeneous condensation

By CAN F. DELALE, GÜNTER H. SCHNERR AND JÜRGEN ZIEREP

Institut für Strömungslehre und Strömungsmaschinen, Universität Karlsruhe (TH), Germany

(Received 20 December 1993 and in revised form 18 August 1994)

The asymptotic solution of shock tube flows with homogeneous condensation is presented for both smooth, or subcritical, flows and flows with an embedded shock wave, or supercritical flows. For subcritical flows an analytical expression, independent of the particular theory of homogeneous condensation to be employed, that determines the condensation wave front in the rarefaction wave is obtained by the asymptotic analysis of the rate equation along pathlines. The complete solution is computed by an algorithm which utilizes the classical nucleation theory and the Hertz–Knudsen droplet growth law. For supercritical flows four distinct flow regimes are distinguished along pathlines intersecting the embedded shock wave analogous to supercritical nozzle flows. The complete global solution for supercritical flows is discussed only qualitatively owing to the lack of a shock fitting technique for embedded shock waves. The results of the computations obtained by the subcritical algorithm show that most of the experimental data available exhibit supercritical flow behaviour and thereby the predicted onset conditions in general show deviations from the measured values. The causes of these deviations are reasoned by utilizing the qualitative global asymptotic solution of supercritical flows.

1. Introduction

The shock tube offers an alternative technique with desirable features in addition to the well-known cloud chamber and nozzle experiments in understanding condensation dynamics. The experimental conditions in this case can be better controlled. The application of the shock tube to study condensation dynamics was initiated by Wegener & Lundquist (1951) and the first streak photographs of the condensation zones were obtained by Glass & Patterson (1955). Since then, shock tube experiments with non-equilibrium condensation taking place in the rarefaction wave have been carried out by various investigators among whom we can cite Courtney (1965), Homer (1971), Kawada & Mori (1973), Barschdorff (1975), Kalra (1975), Lee (1977) and Peters (1987). A detailed analysis for the onset of condensation was presented by Wu (1977) by solving numerically the system of differential equations arising from the condensation rate equation. The solution including the effect of heat addition on the flow field was exhibited by Sislian (1975) using the numerical method of characteristics; however, with the initial conditions chosen for comparison with the experiments of Kalra (1975) the characteristics emanating from the origin were seen to intersect in the heat addition zones, showing clearly the existence of embedded shock waves which were then smoothed out by employing Lax's (1954) method with artificial viscosity. Recently a comprehensive study was carried out by Smolders (1992), (see also Smolders, Niessen & van Dongen 1992), employing the random choice method.

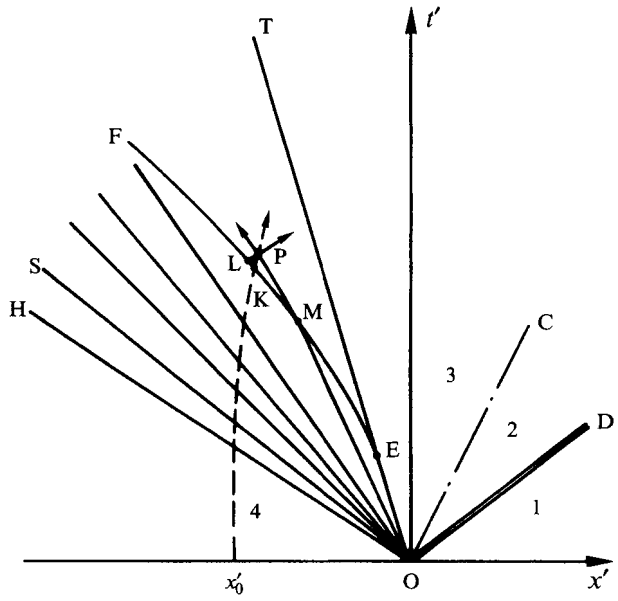

FIGURE 1. Wave diagram for subcritical shock tube flows with non-equilibrium condensation: regions 4 and 1 correspond respectively to the initial states in the driver section and in the channel, OC is the path of the contact surface, OD is the path of shock travelling to the right, OH and OT are respectively the head and tail of the frozen rarefaction wave, OS denotes the locus of those thermodynamic states where saturation is reached, EF is the condensation wave front, OMP and LP are respectively typical left- and right-running characteristics and the dashed line is a typical pathline initially at x'_0.

Unfortunately no attempt to match the theoretical predictions with measurements has been successful. Only some qualitative agreement has been achieved.

It is the purpose of the present investigation to give a full detailed analysis of such flows substantiated by numerical computations. For this reason we consider a mixture of a condensible vapour and a carrier gas which for time $t' < 0$ is at rest in the driver section (region 4 in figure 1) of a shock tube with initial relative humidity φ_4, initial specific humidity ω_4 and initial temperature T'_4. At $t' = 0^+$, just after the diaphragm at $x' = 0$ is instantly removed, the contact surface moves off along the path OC, a shock wave travels to the right along path OD and a rarefaction wave centred at O travels to the left (we herein assume the ideal case of a planar centred expansion wave). The lines OH and OT are respectively the rarefaction wave head and the virtual frozen rarefaction wave tail. The line OS represents the constant thermodynamic state along which saturation is reached. After the rupture of the diaphragm, the mixture suddenly expands into the channel (region 1 in figure 1) and the condensible vapour is cooled in a metastable state reaching relatively high supersaturations until condensation becomes visible (onset of condensation) due to a significant number of droplets formed by homogeneous condensation (heterogeneous condensation is neglected in this consideration). The curve EF in the x'–t' diagram of figure 1 shows a typical wave front for the onset of condensation. The characteristics or waves emanating from point O remain almost straight as long as the effect of homogeneous condensation on the flow variables is negligibly small (negligible heat addition). However, as these characteristics cross the condensation wave front EF of figure 1, they begin to curve appreciably towards the head of the rarefaction wave due to substantial heat addition. Curve OMP shows such a typical characteristic whereas curve LP shows that part of a typical right-running

characteristic in the head addition zones. If the amount of heat added to the flow in the heat addition zones exceeds a critical value, the characteristics emanating from point O may intersect forming embedded shock waves. In this case the condensation front EF of figure 1 may not necessarily represent the onset of condensation as will be discussed in detail in § 5. The essential problem is to locate the condensation wave front EF, to determine the effect of heat addition on the non-stationary flow field and, in the case of an embedded shock, to be able to fit the shock.

In this investigation a detailed asymptotic analysis of the condensation rate equation (coupled to the equations of flow and state) along pathlines is carried out to provide a satisfactory description of shock tube flows with homogeneous condensation (the Riemann problem with non-equilibrium phase transition). The details of the asymptotic method of solving the condensation rate equation in quasi-one-dimensional nozzle flows can be found in Blythe & Shih (1976) and Clarke & Delale (1986). Predictions of the asymptotic method in transonic nozzle flows have recently been given by Delale, Schnerr & Zierep (1993*a*, *b*). At this point, because of the unsteady nature of the flow, it is important to mention that the asymptotic solution of steady quasi-one-dimensional nozzle flows cannot directly be applied along pathlines. However, the mathematical method of solving the rate equation is the same and the same rate laws (nucleation and droplet growth) are employed in both cases (unsteady effects of nucleation and droplet growth, which at best can refine the analytical structure of the condensation zones, are neglected). In spite of the fact that the analytical structure of the condensation zones along pathlines presented here resembles that of quasi-one-dimensional flows (Clarke & Delale 1986), the complete gas dynamical solution along these pathlines possesses the unsteady character of the flow field and is completely different from the one-dimensional steady solution of nozzle flows. In fact the nearly frozen approximations to the onset of condensation and, in the case of embedded shock waves, shock formation are completely different in each flow. It is also worthwhile to mention that in the case of embedded discontinuities such as shock waves, depending on the working fluid and initial conditions, the solution downstream of the shock need not necessarily be a relaxing flow toward thermodynamic equilibrium (e.g. Smolders *et al.* 1992 have shown that condensation behind the discontinuity can be totally quenched and restarted again forming a periodic flow pattern for the case of heterogeneous condensation. Similar flow patterns should not be ruled out for the case of homogeneous condensation with some special conditions at relatively low supersaturations and possibly large times; in such a case, the relaxation solution behind the embedded shock of § 4 should be replaced by the corresponding natural solution governed by the conditions just downstream of the shock).

With these remarks in mind we herein present the global solution for both smooth flows and flows with embedded shock waves (in the latter case only those non-equilibrium flows relaxing toward thermodynamic equilibrium along pathlines downstream of the shock are discussed). Smooth (subcritical) flows are studied both qualitatively and quantitatively whereas flows with embedded shock waves (supercritical flows) are discussed only qualitatively owing to lack of a shock fitting technique. Four distinct supercritical flow regimes along pathlines intersecting the embedded shock wave are distinguished and the global solution is constructed by an assembly of pathlines falling in appropriate supercritical regimes. A subcritical algorithm which exhibits the asymptotic solution in distinct condensation zones along pathlines is developed for the expansion of a mixture of water vapour and a carrier gas in the rarefaction wave. The condensation wave front is precisely located and

compared with the onset conditions of different experiments. Finally the causes of the departure of the asymptotic predictions from the experimental onset conditions are identified and discussed in detail.

2. Basic equations

In this section we discuss the basic equations of condensing shock tube flows in normalized form and cast them into their normalized characteristic form.

2.1. *The flow and state equations*

We consider the equations of motion of unsteady compressible flow of a mixture of a condensible vapour, herein denoted by subscript v, and a carrier gas, denoted by subscript i, in the form

$$\frac{\partial \rho'}{\partial t'} + \frac{\partial}{\partial x'}(\rho' u') = 0, \tag{1}$$

$$\frac{\partial u'}{\partial t'} + u' \frac{\partial u'}{\partial x'} = -\frac{1}{\rho'} \frac{\partial p'}{\partial x'}, \tag{2}$$

$$\frac{\mathrm{d}h'}{\mathrm{d}t'} = \frac{1}{\rho'} \frac{\mathrm{d}p'}{\mathrm{d}t'}, \tag{3}$$

where ρ', p' and u' are respectively the mixture density, the mixture pressure and the flow velocity, t' denotes the time, x' is the axial coordinate along the shock tube with origin at the location of the diaphragm and $\mathrm{d}/\mathrm{d}t'$ denotes the total derivative. The mixture enthalpy h' is defined by

$$h' = c'_{pm} T' - gL', \tag{4}$$

where T' is the temperature, g is the ratio of the mass flow rate of the condensate to that of the mixture, called the condensate mass fraction, L' is the latent heat of condensation and c'_{pm} is the specific heat of the mixture at constant pressure given by

$$c'_{pm} = (1-\omega_4)\, c'_{pi} + \omega_4\, c'_{pv}, \tag{5}$$

with c'_{pi} and c'_{pv} denoting respectively the specific heats at constant pressure of the carrier gas and of the vapour and with ω_4 denoting the initial specific humidity of the vapour in the driver section (see figure 1).

The thermal equation of state of the mixture follows by Dalton's law from the thermal equations of state of the condensible vapour and carrier gas, both taken to be ideal gases, i.e.

$$p' = p'_i + p'_v = \frac{\mathfrak{R}}{\mu_i} \rho'_i T' + \frac{\mathfrak{R}}{\mu_v} \rho'_v T', \tag{6}$$

where $\mathfrak{R}$ is the universal gas constant, μ_i, μ_v are respectively the molecular masses of the carrier gas and condensible vapour, ρ'_i and ρ'_v are respectively the carrier gas and vapour densities related to the mixture density ρ' by the relations

$$\rho'_i = (1-\omega_4)\, \rho' \tag{7}$$

and

$$\rho'_v = (\omega_4 - g)\, \rho'. \tag{8}$$

Equation (6) then takes the form

$$p' = \frac{\mathfrak{R}}{\mu_m} \left(1 - \frac{\mu_m}{\mu_v} g\right) \rho' T', \tag{9}$$

where the mixture molecular mass μ_m is defined by

$$\frac{1}{\mu_m} \equiv \frac{1-\omega_4}{\mu_i} + \frac{\omega_4}{\mu_v}. \tag{10}$$

For convenience we now carry out the normalization

$$p \equiv p'/p'_4, \quad \rho \equiv \rho'/\rho'_4, \quad T \equiv T'/T'_4, \quad u \equiv u'/a'_4 \tag{11}$$

and

$$h \equiv h'/h'_4 = h'/(c'_{pm}\, T'_4), \quad L \equiv L'\mu_v/(\Re T'_4), \tag{12}$$

where a'_4 is the initial speed of sound in the driver section given by

$$a'^2_4 = (\Re/\mu_m)\,\gamma_m\, T'_4 \tag{13}$$

with the mixture adiabatic exponent γ_m defined by

$$\gamma_m \equiv \frac{c'_{pm}}{c'_{pm} - \Re/\mu_m}. \tag{14}$$

The coordinates t' and x' are non-dimensionalized by

$$t \equiv t'/\Theta', \quad x \equiv x'/(a'_4\,\Theta'), \tag{15}$$

where Θ' is some characteristic flow time. The flow and state equations (1), (2), (3) and (9) now assume the normalized form

$$\frac{\partial \rho}{\partial t} + \frac{\partial}{\partial x}(\rho u) = 0, \tag{16}$$

$$\frac{\partial u}{\partial t} + u\frac{\partial u}{\partial x} = -\frac{1}{\gamma_m \rho}\frac{\partial p}{\partial x}, \tag{17}$$

$$\frac{\mathrm{d}h}{\mathrm{d}t} = \frac{(\gamma_m - 1)}{\gamma_m \rho}\frac{\mathrm{d}p}{\mathrm{d}t}, \tag{18}$$

and

$$p = (1 - (\mu_m/\mu_v)\, g)\,\rho T, \tag{19}$$

where

$$h = T - (\mu_m/\mu_v\, c_{pm})\, gL \tag{20}$$

with c_{pm} defined by

$$c_{pm} \equiv c'_{pm}\,\mu_m/\Re = \gamma_m/(\gamma_m - 1), \tag{21}$$

and with $\mathrm{d}/\mathrm{d}t = \partial/\partial t + u\,\partial/\partial x$. The above normalized flow and state equations (16)–(19) do not form a complete system unless they are supplemented by the condensation rate equation for g.

2.2. *The condensation rate equation*

The non-equilibrium condensation rate equation is constructed from a convenient nucleation rate equation together with a droplet growth law (e.g. see Sislian 1975; Sislian & Glass 1976; Wu 1977). If we consider a fluid element at (x', t') on a pathline of figure 1 and assume the droplets formed to be spherical, a droplet of condensate in this element formed at a point (χ', τ') upstream on the same pathline with initial radius (the critical radius for droplet formation) $r'^*(\chi', \tau')$ will grow into its present size r' given by

$$r'(\chi', \tau'; x', t') = r'^*(\chi', \tau') + \int_{\tau'}^{t'} \frac{\mathrm{d}r'}{\mathrm{d}t'}\,\mathrm{d}t', \tag{22}$$

where $\mathrm{d}r'/\mathrm{d}t'$ is the local droplet growth rate of the droplet, assumed to depend only on the local state of the two-phase mixture, and where it is understood that the integration is carried out along the pathline passing through (x', t'). The rate equation for the condensate mass fraction g in the fluid element at (x', t') then follows by definition as

$$g(x', t') = \tfrac{4}{3}\pi\rho'_{con}(x', t') \int_{t'_s}^{t'} [r'(\chi', \tau'; x', t')]^3 \frac{J'(\chi'\tau')}{\rho'(\chi', \tau')} \mathrm{d}\tau' \tag{23}$$

along a pathline where $\mathrm{d}x'/\mathrm{d}t' = u'$. In (23) t'_s is the time when saturation is reached along a pathline, $J'(\chi', \tau')$ is the rate of production of condensation nuclei of critical size per unit time and volume at (χ', τ'), $\rho'_{con}(x', t')$ is the density of the condensate at (x', t') and $r'(\chi', \tau'; x', t')$ is given by (22). A complete physical description of the rate equation (23) now demands that the nucleation rate J' and the droplet growth rate $\mathrm{d}r'/\mathrm{d}t'$ be known. Unfortunately there are no universally accepted theories of these rate laws which one can employ independent of the choice of the condensible vapour. Nevertheless the well-known nucleation theories (Zettlemoyer 1969) suggest that J' can in general be taken to be of the form

$$J' = \zeta' J = \zeta' \Sigma(p, T, g) \exp[-K^{-1} B(p, T, g)], \tag{24}$$

where ζ' is a normalization constant for the nucleation rate, B and Σ are respectively the normalized activation function and the normalized pre-exponential factor of nucleation theories both depending on the local thermodynamic state of the mixture, and K is the nucleation parameter depending only on the initial conditions of the vapour in the driver section and on the choice of the mixture of condensible vapour and carrier gas. Homogeneous nucleation lasting for a relatively long time compared to flow time to reach its peak implies $K \ll 1$. Before we discuss the general form of the droplet growth rate, herein assumed to be independent of the droplet radius, we normalize the droplet radius r' as

$$r \equiv r'/r'_d, \tag{25}$$

where

$$r'_d = \left(\frac{3\rho'_4}{4\pi\bar{\rho}_{con}\zeta'\Theta'}\right)^{1/3} \tag{26}$$

with $\bar{\rho}_{con}$ denoting the mean density of the condensate in the temperature ranges investigated. Using the normalization of the previous section together with (25), the radius independent normalized droplet growth law can be written as

$$\mathrm{d}r/\mathrm{d}t = \lambda\Omega(p, T, g), \tag{27}$$

where Ω is the droplet growth function depending on the thermodynamic state of the mixture and λ is the droplet growth parameter. In particular rapid droplet growth in the rarefaction wave, which corresponds to small droplet growth time compared to characteristic flow time, is characterized by $\lambda \gg 1$. By substituting from (24) for J' and from (27) for $\mathrm{d}r'/\mathrm{d}t'$, and by approximating $\rho'_{con}(x', t')$ by $\bar{\rho}_{con}$ in the operational temperature range, the integral condensation rate equation on pathlines assumes the normalized form

$$g(t) = \int_{t_s}^{t} \left[r^*(\tau) + \lambda \int_{\tau}^{t} \Omega(\eta)\,\mathrm{d}\eta\right]^3 \frac{\Sigma(\tau)\exp[-K^{-1}B(\tau)]}{\rho(\tau)} \mathrm{d}\tau. \tag{28}$$

The above normalized rate equation, as it stands, is coupled to the equations of flow and state of the previous section.

2.3. *The characteristic form of the equations of motion*

Using standard techniques (e.g. see Vincenti & Kruger 1965; Whitham 1974; Sislian 1975), the normalized flow and state equations (16)–(19) can be cast into the characteristic form

$$\left(1-\frac{\mu_m}{\mu_v}g\right)\mathrm{d}\ln p \pm \frac{\gamma_m a_f}{T}\mathrm{d}u + \frac{\mu_m[c_{pm}-gL_1\mu_m/\mu_v-(1-g\mu_m/\mu_v)L/T]}{\mu_v[c_{pm}-1+(1-L_1)g\mu_m/\mu_v]}\chi\,\mathrm{d}t = 0 \quad (29)$$

on $\mathrm{d}x/\mathrm{d}t = u \pm a_f$ and

$$\left(1-\frac{\mu_m}{\mu_v}g\right)\mathrm{d}\ln p - \left(c_{pm}-\frac{\mu_m}{\mu_v}gL_1\right)\mathrm{d}\ln T + \frac{\mu_m L}{\mu_v T}\chi\,\mathrm{d}t = 0 \quad (30)$$

on $\mathrm{d}x/\mathrm{d}t = u$, where the function χ is defined by

$$\chi \equiv \mathrm{d}g/\mathrm{d}t, \quad (31)$$

$L_1 \equiv \mathrm{d}L/\mathrm{d}T$ and a_f is the normalized (with respect to a_4') local frozen speed of sound given by

$$a_f^2 \equiv \frac{(c_{pm}-1)(c_{pm}-gL_1\mu_m/\mu_v)(1-g\mu_m/\mu_v)}{c_{pm}\quad(c_{pm}-1+(1-L_1)g\mu_m/\mu_v)}T. \quad (32)$$

On the other hand the integral rate equation (28) is already in characteristic form (i.e. $g = g(t)$ on $\mathrm{d}x/\mathrm{d}t = u$). Thus (28), (29) and (30) together with the thermal equation of state (19) form a complete set for the solution of shock tube flows with homogeneous condensation. It is worthwhile to mention that for frozen flows ($g \equiv 0$), (29) yields constant Riemann invariants ($R_\pm = 2a_f/(\gamma_m-1) \pm u = \text{constant}$) on the characteristics $\mathrm{d}x/\mathrm{d}t = u \pm a_f$ and (30) reduces to the classical isentropic relation ($p \propto T^{\gamma_m/(\gamma_m-1)}$).

3. Asymptotic solution of subcritical or smooth flows

In this section we present the asymptotic solution of the rate equation (28) along pathlines in the double limit as $K \to 0$ and $\lambda \to \infty$ characterizing respectively large nucleation time and small droplet growth time compared to the characteristic flow time. In this case the behaviour of the activation function $B = B(t)$ distinguishes the distinct condensation zones along pathlines. A typical variation of the activation function B along a pathline with distinct condensation zones is shown in figure 2. For $t \leqslant t_s$, with t_s corresponding to the time when the saturation line in the p_v–T diagram of the vapour is traversed, B is infinite (vanishing nucleation rate). At $t = t_l$, called the 'relative onset point', B exhibits an absolute minimum $[(\mathrm{d}B/\mathrm{d}t)_{t=t_l} = 0]$ corresponding to a maximum nucleation rate which marks the end of the empirical onset of condensation. The distinct condensation zones along any pathline then follow from the corresponding behaviour of the activation function before and after the onset of condensation.

3.1. *To onset of condensation from initial growth*

This is the region which occurs in the interval $t_s \leqslant t \leqslant t_l$ along any pathline and is dominated by the production of condensation nuclei that peaks at $t = t_l$. Herein four physically distinct (only two are asymptotically distinct) condensation zones can be distinguished. These are the initial growth zone (IGZ), further growth zone (FGZ), the rapid growth zone (RGZ) and the onset zone (OZ). Of these four physically distinct condensation zones, to be defined below, the first two and the last two are not asymptotically distinct. Thus the asymptotic analysis of the rate equation for these zones can be carried out in a combined fashion. The initial and further growth zones are defined as those zones where $\mathrm{d}B/\mathrm{d}t = O(1)$. They are distinguished physically. In

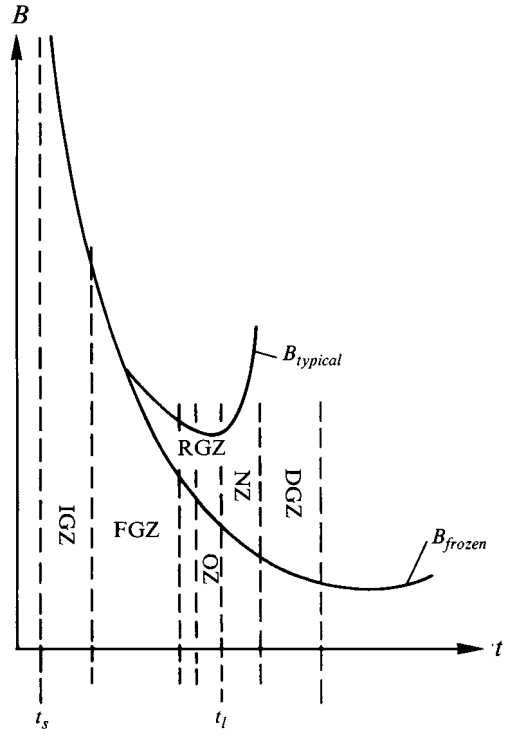

FIGURE 2. The variation of the normalized activation function B along a typical pathline exhibiting the physically distinct condensation zones in subcritical flows.

the initial growth zone (IGZ), $B = B_f$, where B_f denotes the frozen activation function with $g \equiv 0$. The further growth zone (FGZ) is distinguished as the zone where small deviations of B from B_f start to occur with $\mathrm{d}B/\mathrm{d}t$ still of $O(1)$. However, since these two zones are not asymptotically distinct, the asymptotic solution of the rate equation (28) along any chosen pathline applies to both zones. This follows uniquely using Laplace's method (see Erdelyi 1956; Sirovich 1971) for an end point minimum in the double limit as $K \to 0$ and $\lambda \to \infty$. The resulting expressions for g and $\mathrm{d}g/\mathrm{d}t$ in these zones, obtained following the asymptotic procedure given in Delale *et al.* (1993*a*), are

$$g(t) = \frac{\Sigma(t)}{\rho(t)} K^4 \left(\frac{\mathrm{d}B}{\mathrm{d}t}\right)^{-4} \exp\left[-K^{-1}B(t)\right] \times \left\{6\lambda^3\Omega^3(t) - 6\lambda^2\Omega^2(t)\left[\frac{r^*(t)\,\mathrm{d}B/\mathrm{d}t}{K}\right] + 3\lambda\Omega(t)\left[\frac{r^*(t)\,\mathrm{d}B/\mathrm{d}t}{K}\right]^2 - \left[\frac{r^*(t)\,\mathrm{d}B/\mathrm{d}t}{K}\right]^3\right\}, \tag{33}$$

$$\frac{\mathrm{d}g}{\mathrm{d}t} = -\frac{\Sigma(t)}{\rho(t)} K^3 \left(\frac{\mathrm{d}B}{\mathrm{d}t}\right)^{-3} \exp\left[-K^{-1}B(t)\right] \times \left\{6\lambda^3\Omega^3(t) - 6\lambda^2\Omega^2(t)\left[\frac{r^*(t)\,\mathrm{d}B/\mathrm{d}t}{K}\right] + 3\lambda\Omega(t)\left[\frac{r^*(t)\,\mathrm{d}B/\mathrm{d}t}{K}\right]^2 - \left[\frac{r^*(t)\,\mathrm{d}B/\mathrm{d}t}{K}\right]^3\right\}, \tag{34}$$

with $\mathrm{d}B/\mathrm{d}t$ given by

$$\frac{\mathrm{d}B}{\mathrm{d}t} = \frac{\partial B}{\partial p}\frac{\mathrm{d}p}{\mathrm{d}t} + \frac{\partial B}{\partial T}\frac{\mathrm{d}T}{\mathrm{d}t} + \frac{\partial B}{\partial g}\frac{\mathrm{d}g}{\mathrm{d}t} \tag{35}$$

along a pathline.

The rapid growth (RGZ) and onset (OZ) zones are defined as those zones where $\mathrm{d}B/\mathrm{d}t$ diminishes to $O(K^{1/2})$ as $K \to 0$ along a pathline. The 'relative onset point' $t = t_l$ where $\mathrm{d}B/\mathrm{d}t \equiv 0$ marks the end of the onset of condensation. In fact the onset zone (OZ), which contains the empirical onset point, can be regarded as being embedded in RGZ just upstream of the relative onset point t_l (figure 2). The asymptotic expressions for g and its derivatives $\mathrm{d}g/\mathrm{d}t$ and $\mathrm{d}^2g/\mathrm{d}t^2$ in these zones follow from (28) using Laplace's method for an end-point minimum (for details of the asymptotic method, see e.g. Delale *et al.* 1993*a*):

$$\begin{aligned} g(t) = {} & \frac{\Sigma(t)}{\rho(t)}[2\beta(t)]^{-2}\left(\exp\left[\frac{\gamma^2(t)}{8\beta(t)}\right]\right)\exp[-K^{-1}B(t)] \\ & \times\left\{6\lambda^3\Omega^3(t)\,D_{-4}\left[\frac{\gamma(t)}{(2\beta(t))^{1/2}}\right] + 6\lambda^2(t)\,\Omega^2(t)\,[r^*(t)\,(2\beta(t))^{1/2}]\,D_{-3}\left[\frac{\gamma(t)}{(2\beta(t))^{1/2}}\right]\right. \\ & \left. + 3\lambda\Omega(t)\,[r^*(t)\,(2\beta(t))^{1/2}]^2\,D_{-2}\left[\frac{\gamma(t)}{(2\beta(t))^{1/2}}\right] + [r^*(t)\,(2\beta(t))^{1/2}]^3\,D_{-1}\left[\frac{\gamma(t)}{(2\beta(t))^{1/2}}\right]\right\}, \end{aligned} \tag{36}$$

$$\begin{aligned} \frac{\mathrm{d}g}{\mathrm{d}t} = {} & \frac{\Sigma(t)}{\rho(t)}[2\beta(t)]^{-3/2}\left(\exp\left[\frac{\gamma^2(t)}{8\beta(t)}\right]\right)\exp[-K^{-1}B(t)] \\ & \times\left\{6\lambda^3\Omega^3(t)\,D_{-3}\left[\frac{\gamma(t)}{(2\beta(t))^{1/2}}\right] + 6\lambda^2\Omega^2(t)\,[r^*(t)\,(2\beta(t))^{1/2}]\,D_{-2}\left[\frac{\gamma(t)}{(2\beta(t))^{1/2}}\right]\right. \\ & \left. + 3\lambda\Omega(t)\,[r^*(t)\,(2\beta(t))^{1/2}]^2\,D_{-1}\left[\frac{\gamma(t)}{(2\beta(t))^{1/2}}\right] + [r^*(t)\,(2\beta(t))^{1/2}]^3\exp\left[-\frac{\gamma^2(t)}{8\beta(t)}\right]\right\}, \end{aligned} \tag{37}$$

$$\begin{aligned} \frac{\mathrm{d}^2g}{\mathrm{d}t^2} = {} & \frac{1}{\Omega(t)}\frac{\mathrm{d}\Omega}{\mathrm{d}t}\frac{\mathrm{d}g}{\mathrm{d}t} + \frac{\Sigma(t)}{\rho(t)}[2\beta(t)]^{-1}\left(\exp\left[\frac{\gamma^2(t)}{8\beta(t)}\right]\right)\exp[-K^{-1}B(t)] \\ & \times\left\{6\lambda^3\Omega^3(t)\,D_{-2}\left[\frac{\gamma(t)}{(2\beta(t))^{1/2}}\right] + 6\lambda^2(t)\,\Omega^2(t)\,[r^*(t)\,(2\beta(t))^{1/2}]\,D_{-1}\left[\frac{\gamma(t)}{(2\beta(t))^{1/2}}\right]\right. \\ & + 3\lambda\Omega(t)\,[r^*(t)\,(2\beta(t))^{1/2}]^2\exp\left[-\frac{\gamma^2(t)}{8\beta(t)}\right] + [r^*(t)\,(2\beta(t))^{1/2}]^3\exp\left[-\frac{\gamma^2(t)}{8\beta(t)}\right] \\ & \left.\times\left[\frac{3}{r^*(t)}\frac{\mathrm{d}r^*}{\mathrm{d}t} + \frac{1}{\Sigma(t)}\frac{\mathrm{d}\Sigma}{\mathrm{d}t} + \gamma(t) - \frac{1}{\rho(t)}\frac{\mathrm{d}\rho}{\mathrm{d}t} - \frac{1}{\Omega(t)}\frac{\mathrm{d}\Omega}{\mathrm{d}t}\right]\Big/(2\beta(t))^{1/2}\right\}, \end{aligned} \tag{38}$$

where

$$\gamma(t) \equiv -K^{-1}\,\mathrm{d}B/\mathrm{d}t \geqslant 0, \tag{39}$$

$$\beta(t) \equiv \tfrac{1}{2}K^{-1}\,\mathrm{d}^2B/\mathrm{d}t^2 > 0 \tag{40}$$

with $\mathrm{d}B/\mathrm{d}t$ to be evaluated from (35) and $\mathrm{d}^2B/\mathrm{d}t^2$ given by

$$\begin{aligned} \frac{\mathrm{d}^2B}{\mathrm{d}t^2} = {} & \frac{\partial B}{\partial p}\frac{\mathrm{d}^2p}{\mathrm{d}t^2} + \frac{\partial B}{\partial T}\frac{\mathrm{d}^2T}{\mathrm{d}t^2} + \frac{\partial B}{\partial g}\frac{\mathrm{d}^2g}{\mathrm{d}t^2} + \frac{\partial^2 B}{\partial p^2}\left(\frac{\mathrm{d}p}{\mathrm{d}t}\right)^2 + \frac{\partial^2 B}{\partial T^2}\left(\frac{\mathrm{d}T}{\mathrm{d}t}\right)^2 \\ & + \frac{\partial^2 \mathrm{B}}{\partial g^2}\left(\frac{\mathrm{d}g}{\mathrm{d}t}\right)^2 + 2\left(\frac{\partial^2 B}{\partial p\,\partial T}\frac{\mathrm{d}p}{\mathrm{d}t}\frac{\mathrm{d}T}{\mathrm{d}t} + \frac{\partial^2 B}{\partial p\,\partial g}\frac{\mathrm{d}p}{\mathrm{d}t}\frac{\mathrm{d}g}{\mathrm{d}t} + \frac{\partial^2 B}{\partial T\,\partial g}\frac{\mathrm{d}T}{\mathrm{d}t}\frac{\mathrm{d}g}{\mathrm{d}t}\right), \end{aligned} \tag{41}$$

and where $D_{-n}(z)$, $n = 1, 2, 3, 4$, is Whittaker's parabolic cylinder function of z (see Abramowitz & Stegun 1965; Gradshteyn & Ryzhik 1980). In particular the asymptotic expressions for g and its derivatives at t_l, where by subscript l we mean 'evaluated at $t = t_l$', can simply be obtained in the limit

$$\gamma \to \gamma_l \equiv 0; \quad \beta \to \beta_l; \quad \Sigma \to \Sigma_l; \text{etc.} \tag{42}$$

Having described the asymptotic solution of the rate equation (28) along a pathline in the characteristic condensation zones from initial growth to onset, we are now in a position to discuss the solution of the flow field in these zones. For this reason we introduce *nearly frozen flows* as those flows which show negligible influence of non-equilibrium condensation on the flow field (weak coupling between the flow equations (16)–(19) and the condensation rate equation (28)). Thus for nearly frozen flows the solution for the flow field at a point (x, t) located in the rarefaction wave is given in the first approximation by the classical isentropic solution

$$p_f(x,t) = \left[1 - \frac{(\gamma_m - 1)}{(\gamma_m + 1)}\left(\frac{x}{t} + 1\right)\right]^{2\gamma_m/(\gamma_m - 1)}. \tag{43}$$

$$u_f(x,t) = \frac{2}{\gamma_m + 1}\left[\frac{x}{t} + 1\right], \tag{44}$$

$$a_{fo}^2(x,t) = T_f(x,t) = [p_f(x,t)]^{(\gamma_m - 1)/\gamma_m}, \tag{45}$$

and

$$\rho_f(x,t) = [p_f(x,t)]^{1/\gamma_m}, \tag{46}$$

where subscript f denotes the frozen (isentropic) values with $g \equiv 0$ (the normalized frozen speed of sound at $g \equiv 0$ is herein distinguished by subscript fo from its local frozen value at fixed g given by (32)). The equation for pathlines in nearly frozen flows can now, as a first approximation, be taken as

$$\frac{x}{t} = \frac{1}{(\gamma_m - 1)}\left[2 - (\gamma_m + 1)\left(\frac{t_0}{t}\right)^{(\gamma_m - 1)/(\gamma_m + 1)}\right], \tag{47}$$

where t_0 is the normalized time when the rarefaction wave head reaches the initial position x_0 of the pathline.

In the initial growth zone (IGZ), $B = B_f$ by definition and all other thermodynamic functions assume their frozen values, i.e. $\Sigma = \Sigma_f$, $\Omega = \Omega_f$, etc. Thus in this zone the flow field can be evaluated exactly from the frozen solution given above by (43)–(47), and a complete decoupling of the rate equation from the flow and state equations is possible. The initial growth of the condensate mass fraction g and its total derivative $\mathrm{d}g/\mathrm{d}t$ can in turn be explicitly evaluated from (33) and (34) respectively by replacing all of the thermodynamic functions by their frozen values. In all of the remaining zones, FGZ, RGZ and OZ, the solution can be obtained iteratively starting with the frozen solution. Owing to the weak coupling between the condensation rate equation and the flow equations in nearly frozen flows, the frozen solution of (43)–(47) will not be significantly altered in these zones. Thus as a first approximation the solution of (43)–(47) can be assumed to hold in these zones as well (small deviations from this solution can occur especially in the onset zone (OZ). These deviations can, in principle, be taken into account by iteration using the characteristic equations (29) and (30) locally; however, such an iteration is normally not necessary since the onset zone has relatively small thickness). On the other hand the activation function B and its total derivatives will deviate from their frozen values appreciably especially in RGZ and OZ.

Consequently g and its total derivatives cannot be evaluated using the frozen values of B and its total derivatives. Thus a local iterative procedure is necessary to evaluate g and its derivatives in FGZ, RGZ and OZ. This iteration scheme is fairly simple. On any pathline of our choice and at any particular time t falling in one of the above zones, we first use the frozen solution to evaluate g and its total derivatives from (33) and (34) in FGZ and from (36)–(38) in RGZ and OZ. Using these values, we correct for the thermodynamic functions, in particular for B and its total derivatives $\mathrm{d}B/\mathrm{d}t$ and $\mathrm{d}^2B/\mathrm{d}t^2$. Substitution of these corrected values into (33) and (34) in FGZ and into (36)–(38) in RGZ and OZ yields the new iterates of g and its total derivatives. Iteration ends when the successive iterative values for g and its total derivatives are close enough to each other (normally a single iteration suffices). Using this iterative scheme the asymptotic solution in each of the zones FGZ, RGZ and OZ can be exhibited along any pathline of our choice. In particular the relative onset point, which marks the end of the onset zone with a maximum nucleation rate, on any pathline can now be identified as the point where

$$\left(\frac{\mathrm{d}B}{\mathrm{d}t}\right)_{t=t_l} = 0. \tag{48}$$

Repeating the procedure for different pathlines, we can construct the locus of the relative onset points which we will refer to as *the condensation wave front* (curve EF in figure 1).

3.2. *Heat addition by homogeneous condensation*

Following the onset of condensation on a pathline, i.e. downstream of the onset zone ($t \geqslant t_l$), the effect of heat added to the flow can no longer be neglected and the asymptotic solution presented above for nearly frozen flows becomes invalid. Heat addition to the flow on a pathline downstream of the onset zone essentially occurs in two asymptotically and physically distinct zones distinguished from the asymptotic solution of the condensation rate equation (28). These are the nucleation zone with growth (NZ) where both nucleation and droplet growth are important and the droplet growth zone (DGZ) which is dominated solely by droplet growth with practically vanishing nucleation rate (see figure 2). The nucleation zone with growth (NZ) starts at $t = t_l$ where the nucleation rate is maximum (B is minimum) and extends downstream on a pathline until nucleation becomes negligible for any practical purpose. A considerable amount of heat begins to be set free in this zone giving rise to increases in the pressure, density and temperature of the mixture over a short time interval. Using Laplace's method for an interior minimum at $t = t_l$, the condensation rate equation (28) in this zone along a particular pathline yields

$$g = b_l[(r_l^* + a_l\phi)^3 F_0(\phi) - 3a_l(r_l^* + a_l\phi)^2\, F_1(\phi) + 3a_l^2(r_l^* + a_l\phi)\, F_2(\phi) - a_l^3 F_3(\phi)], \tag{49}$$

$$\chi \equiv \frac{\mathrm{d}g}{\mathrm{d}t} = r^{*3}(t)\frac{\Sigma(t)\exp[-K^{-1}B(t)]}{\rho(t)} + 3\lambda\Omega(t)\, b_l[(r_l^* + a_l\phi)^2 F_0(\phi) - 2a_l(r_l^* + a_l\phi)\, F_1(\phi) + a_l^2 F_2(\phi)], \tag{50}$$

where

$$a_l \equiv \lambda\Omega_l\beta_l^{-1/2} \tag{51}$$

$$b_l \equiv \frac{\Sigma_l}{\rho_l}\beta_l^{-1/2}\exp[-K^{-1}B_l], \tag{52}$$

the stretched coordinate ϕ is given by

$$\phi \equiv \beta_l^{1/2}(t - t_l) \geqslant 0, \tag{53}$$

and the functions $F_k(\phi)$ $(k = 0, 1, 2, 3)$ are defined by

$$F_0(\phi) \equiv \tfrac{1}{2}\pi^{1/2}(1 + \operatorname{erf}\phi), \tag{54}$$

$$F_1(\phi) \equiv -\tfrac{1}{2}e^{-\phi^2}, \tag{55}$$

$$F_2(\phi) \equiv \tfrac{1}{4}\pi^{1/2}(1 + \operatorname{erf}\phi) - \tfrac{1}{2}\phi\, e^{-\phi^2}, \tag{56}$$

$$F_3(\phi) \equiv -\tfrac{1}{2}(\phi^2 + 1)\, e^{-\phi^2}, \tag{57}$$

with $\operatorname{erf}\phi$ denoting the conventional error function of ϕ. In particular as $\phi \to \infty$, the asymptotic expressions for (49) and (50) reduce to

$$g \sim \pi^{1/2} b_l a_l^3 \{\phi^3 + 3(r_l^*/a_l)\phi^2 + 3[\tfrac{1}{2} + (r_l^*/a_l)^2]\phi + (r_l^*/a_l)^3 + \tfrac{3}{2}(r_l^*/a_l)\} \tag{58}$$

and

$$\chi \equiv \frac{dg}{dt} \sim 3\pi^{1/2} \lambda \Omega(t)\, b_l a_l^2 [\phi^2 + 2(r_l^*/a_l)\phi + (r_l^*/a_l)^2 + \tfrac{1}{2}]. \tag{59}$$

These expressions, which correspond to linear growth of the droplet radius with time, cannot persist far downstream of this zone (i.e. in the droplet growth zone (DGZ)) where the two-phase mixture relaxes towards saturated equilibrium states. For this reason in the droplet growth zone we conveniently define a new normalized droplet radius by

$$R \equiv \int_{t_l}^{t} \frac{\Omega(\eta)}{\Omega_l} d\eta \tag{60}$$

together with the scaling variables

$$\bar{R} \equiv \Lambda K^{-1/3} R, \tag{61}$$

$$\theta \equiv \Lambda K^{-1/3}(t - t_l) \tag{62}$$

with

$$\Lambda \equiv (\pi^{1/2} b_l K)^{1/3} \lambda \Omega_l. \tag{63}$$

Now using Laplace's method for an interior minimum at $t = t_l$ in the double limit as $K \to 0$ and $\lambda \to \infty$ together with the limit of vanishing nucleation rate, the condensation rate equation (28) yields

$$g = \bar{R}^3 + \epsilon_2 \bar{R}^2 + \epsilon_1 \bar{R} + \epsilon_0, \tag{64}$$

$$\chi \equiv \frac{dg}{dt} = (\pi^{1/2} b_l)^{1/3} \lambda \Omega(t) [3\bar{R}^2 + 2\epsilon_2 \bar{R} + \epsilon_1], \tag{65}$$

where

$$\epsilon_0 \equiv [r_l^{*3} + \tfrac{3}{2} a_l^2 r_l^*] \pi^{1/2} b_l, \tag{66}$$

$$\epsilon_1 \equiv 3[r_l^{*2} + \tfrac{1}{2} a_l^2] (\pi^{1/2} b_l)^{2/3}, \tag{67}$$

$$\epsilon_2 \equiv 3 r_l^* (\pi^{1/2} b_l)^{1/3}, \tag{68}$$

and where $\bar{R}$ satisfies the relaxation rate equation

$$d\bar{R}/d\theta = \bar{\Omega} \equiv \Omega/\Omega_l \tag{69}$$

together with the initial condition

$$\bar{R} = 0 \quad \text{at} \quad \theta = 0. \tag{70}$$

With the asymptotic expressions given above for g and its total derivative dg/dt along pathlines in the heat addition zones (NZ and DGZ), we are now in a position to present a semi-analytical solution for the flow field in these zones. The analytical

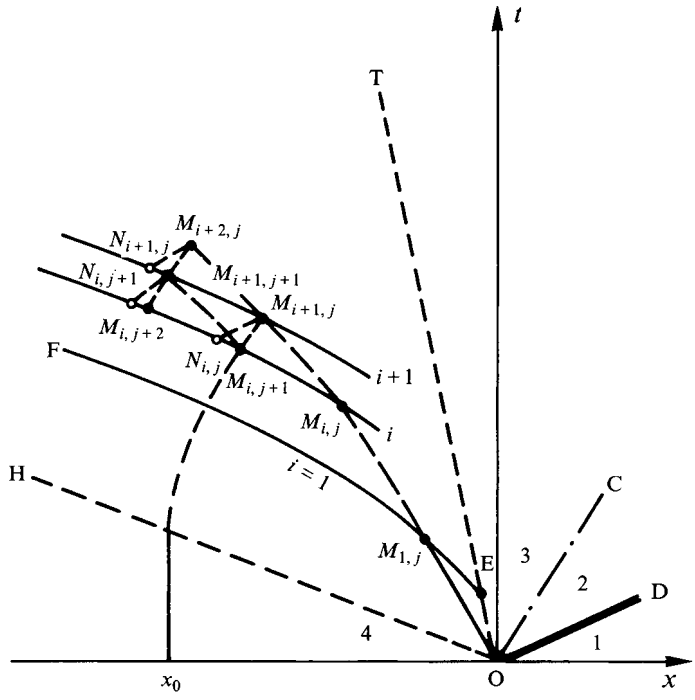

FIGURE 3. Construction scheme for the global solution of subcritical flows in the heat addition zones.

nature of the solution in these zones follows from the analytical expressions for g and its total derivative $\mathrm{d}g/\mathrm{d}t$ obtained from the asymptotic solution of the rate equation (28). The flow field in these zones is obtained by combining the asymptotic expressions (49) and (50) in NZ and (64) and (65) together with (69) in DGZ with the characteristic equations (29) and (30) and solving numerically. Let $M_{i,j}$, $j = 1, 2, 3, \ldots$ be points in the heat addition zone along a given curve i in the x–t plane where the solution for the flow field is known (see figure 3; the starting curve $i = 1$ can be taken as the condensation wave front constructed in the previous subsection). The aim is to locate the set of points $M_{i+1,j}$ on the $(i+1)$th curve to be constructed by interpolation and evaluate the local flow field at these points. Using (29) with the $-$ sign along $M_{i,j}M_{i+1,j}$ where $\mathrm{d}x/\mathrm{d}t = u - a_f$, (29) with the $+$ sign along $N_{i,j}M_{i+1,j}$ where $\mathrm{d}x/\mathrm{d}t = u + a_f$, and (30) on $M_{i,j+1}M_{i+1,j}$ where $\mathrm{d}x/\mathrm{d}t = u$ in finite difference form, and the local asymptotic expressions (49) and (50) if $M_{i,j}$ is in NZ and (64) and (65) together with (69) if $M_{i,j}$ is in DGZ, we arrive at the solution of the flow field (p, T, u and g) at $M_{i+1,j}$ together with the coordinates of the points $N_{i,j}$ and $M_{i+1,j}$ by solving iteratively starting with the solution at points $M_{i,j}$ and $M_{i,j+1}$. Repeating the procedure from $j = 1$ to some integer of our choice, we find the solution for the flow field at points $M_{i+1,j}$; $j = 1, 2, \ldots$ together with their locations in the (x, t)-plane. Starting with $i = 1$ (the condensation wave front) and carrying the same procedure with increasing i until complete relaxation of the rate equation (69) is achieved, we obtain the semi-analytical solution of the flow field in the zones NZ and DGZ.

4. Flows with embedded shock waves (supercritical flows)

The semi-analytical asymptotic solution of subcritical or smooth flows presented in the previous section is in general valid for shock-free flows where the amount of heat added to the flow does not exceed a critical value. When the initial conditions in the driver section are such that this critical amount of heat is exceeded in the heat addition zones along a pathline, the left-running characteristics intersect in these zones. Thus the subcritical solution is no longer valid and should be supplemented by embedded shock waves arising from compressive effects due to heat addition. In this case four distinct supercritical flow regimes (similar supercritical flow regimes are also encountered in steady nozzle flows which can be found in Delale *et al.* 1993*b*) can be distinguished depending on the shock location (z, t_z) along a pathline in the (x, t)-plane (figure 4*a–d*). In Regime I shown in figure 4(*a*) the embedded shock wave falls in FGZ where $\mathrm{d}B/\mathrm{d}t = O(1)$ and the OZ, which contains the empirical onset point and also acts as a precompression zone due to the enormous amount of heat released by condensation in this case, is naturally embedded in FGZ. The excessive heat in this regime is added to the flow downstream of the shock in the zones NZ and DGZ (now structured differently). In Regime II the shock is embedded in RGZ where $\mathrm{d}B/\mathrm{d}t = O(K^{1/2})$ with an OZ which is located just upstream of the shock location along any pathline and which now acts as a weak precompression wave (figure 4*b*). The main heat addition zones NZ and DGZ are again located downstream of the shock on any pathline. Finally in Regimes III and IV the shock falls in the heat addition zones NZ and DGZ respectively (figure 4*c*, *d*). Normally strong embedded shock waves occur in Regime I whereas Regimes III and IV have weak embedded shock waves.

Before we discuss the complete solution, we first notice that the condensation rate equation (28) and thereby its asymptotic solution along a pathline is valid only upstream of the shock location when an embedded shock wave is encountered. Denoting by subscript 1 the thermodynamic functions upstream of the shock location $(t \leqslant t_z)$ and by subscript 2 the same functions downstream of the shock location $(t \geqslant t_z)$ along a pathline, the condensation rate equation (28) should be replaced by

$$g_2(t) = \int_{t_s}^{t_z}\left[r_1^*(\tau) + \lambda\int_{\tau}^{t_z}\Omega_1(\eta)\,\mathrm{d}\eta + \lambda\int_{t_z}^{t}\Omega_2(\eta)\,\mathrm{d}\eta\right]^3\frac{\Sigma_1(\tau)}{\rho_1(\tau)}\exp\left[-K^{-1}B_1(\tau)\right]\mathrm{d}\tau$$
$$+\int_{t_z}^{t}\left[r_2^*(\tau) + \lambda\int_{\tau}^{t}\Omega_2(\eta)\,\mathrm{d}\eta\right]^3\frac{\Sigma_2(\tau)}{\rho_2(\tau)}\exp\left[-K^{-1}B_2(\tau)\right]\mathrm{d}\tau \quad (71)$$

along any pathline for $t \geqslant t_z$. It can be demonstrated from (28) and (71) that $g(t)$ is continuous, but not differentiable at $t = t_z$. The continuity of g is a consequence of the assumption that the droplets pass through the shock unaltered. By denoting by subscripts + and − respectively the states as $t \to t_z^+$ and $t \to t_z^-$, we can show that the shock relation for $\mathrm{d}g/\mathrm{d}t$ takes the form

$$\left(\frac{\mathrm{d}g}{\mathrm{d}t}\right)_+ = \frac{\Omega_+}{\Omega_-}\left(\frac{\mathrm{d}g}{\mathrm{d}t}\right)_- - r_-^{*3}\frac{\Omega_+}{\Omega_-}\frac{\Sigma_-}{\rho_-}\exp\left[-K^{-1}B_-\right] + r_+^{*3}\frac{\Sigma_+}{\rho_+}\exp\left[-K^{-1}B_+\right]. \quad (72)$$

The asymptotic solution of the rate equation (71) along any pathline in each supercritical flow regime follows the same mathematical method as the corresponding supercritical flow regime of nozzle flows by Delale *et al.* (1993*b*). In fact the asymptotic expressions for g presented for the main heat addition zones (NZ and DGZ) downstream of the embedded shock in each supercritical regime of nozzle flows

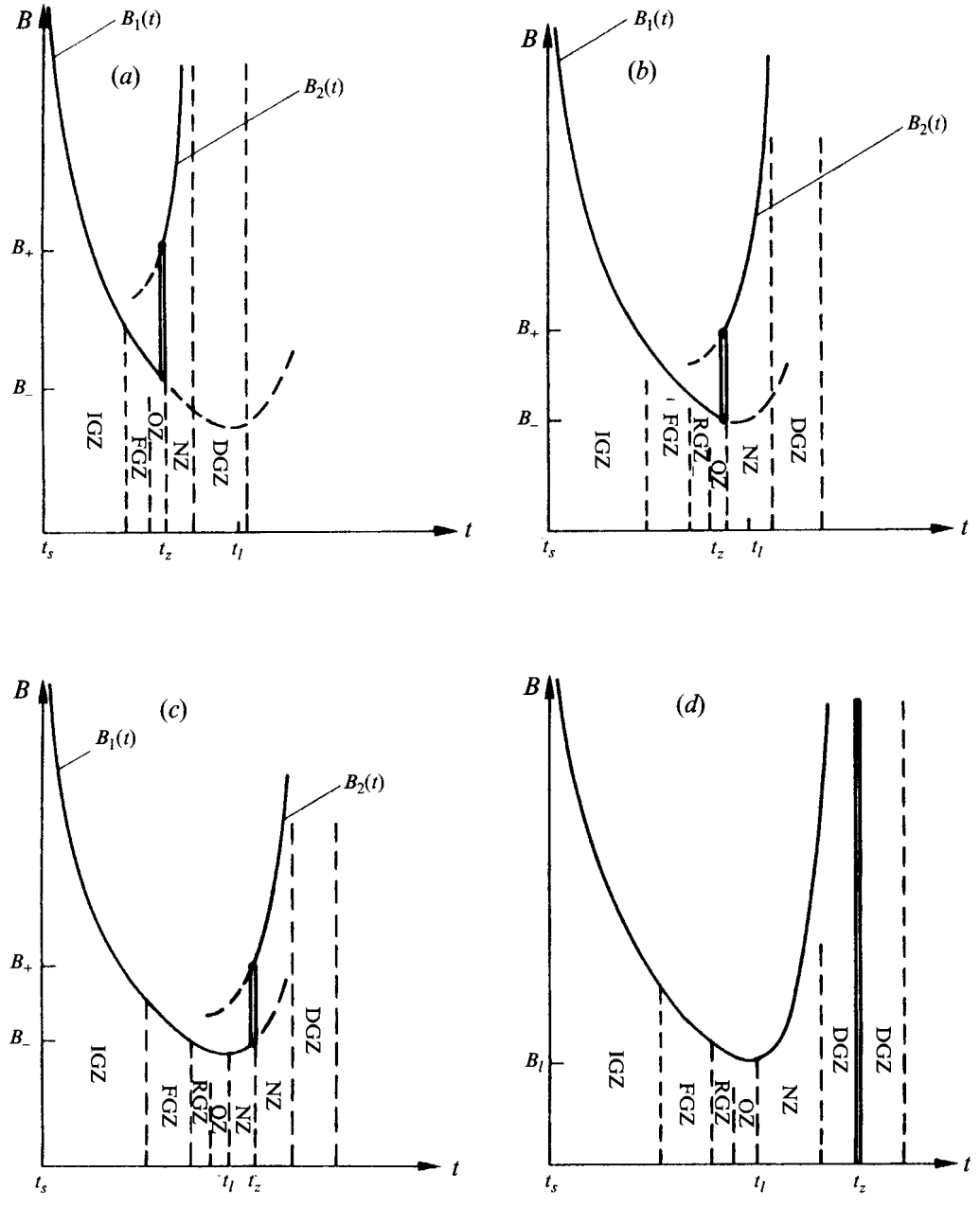

FIGURE 4. Variation of the normalized activation function B along pathlines in distinct supercritical flow regimes and the characteristic condensation zones: (*a*) regime I, (*b*) regime II, (*c*) regime III, and (*d*) regime IV.

remain exactly the same as those in the corresponding zones (NZ and DGZ) of each regime downstream of the shock along any pathline if the normalized nozzle coordinate x is replaced by the normalized time t, if the normalized nozzle area A_z at the shock location is replaced by $1/\rho_-$ or by $1/\rho_+$ depending on whether the corresponding term has resulted from the first or second integral of (71), and if $\mathrm{d}B/\mathrm{d}x$ is replaced by $\mathrm{d}B/\mathrm{d}t$ (we find no basis to present these lengthy expressions herein;

however, these expressions should not physically be interpreted as those of steady nozzle flows for the reasons given in the Introduction). The asymptotic expressions for the derivatives $\chi \equiv \mathrm{d}g/\mathrm{d}t$ can be worked out in exactly the same manner. Thus the asymptotic solution of the rate equation is readily available for the heat addition zones of supercritical flows in each regime.

To be able to discuss, at least qualitatively, the solution of condensing shock tube flows with embedded shock waves, we should also exhibit the shock relations at $t = t_z$ along any pathline. These relations follow from the normalized equations (16)–(18) written in conservation form (e.g. see Whitham 1974):

$$\rho_+ v_+ = \rho_- v_-, \tag{73}$$

$$p_+/\gamma_m + \rho_+ v_+^2 = p_-/\gamma_m + \rho_- v_-^2, \tag{74}$$

and

$$\frac{T_+}{(\gamma_m - 1)} + \tfrac{1}{2}v_+^2 = \frac{T_-}{(\gamma_m - 1)} + \tfrac{1}{2}v_-^2 + \frac{\mu_m}{\mu_v \gamma_m} g_z [L(T_+) - L(T_-)], \tag{75}$$

where v is the normalized flow velocity in a frame where the shock is at rest given by

$$v = u - U, \tag{76}$$

with U denoting the normalized shock velocity (with respect to a_4') and where the subscripts + and − denote respectively the values of the discontinuous variables just downstream and just upstream of the shock location (if a variable is continuous at the shock location along a pathline, its value at the shock location is denoted by subscript z). The shock relations (73)–(75) together with the thermal equation of state at the shock location

$$\frac{p_+}{\rho_+ T_+} = \frac{p_-}{\rho_- T_-} = 1 - \frac{\mu_m}{\mu_v} g_z \tag{77}$$

can be solved implicitly in an iterative manner for the variables just behind the shock (i.e. for p_+, T_+, ρ_+ and v_+) in terms of those just in front of the shock along any pathline provided that the shock velocity U is known (shock fitting).

Having exhibited the local asymptotic solution with embedded shock waves along pathlines on the assumption that we can fit the shock, we now discuss the global solution qualitatively. Embedded shock waves due to excessive heat addition by condensation may appear in the rarefaction wave depending on the initial conditions in the driver section and in the channel or driven section. If these initial conditions are such that the heat released in the heat addition zones is not sufficient to force the left-running characteristics to intersect, the flow remains subcritical everywhere and the global solution is obtained by following the local asymptotic solution of §3 on each pathline entering the rarefaction wave. These type of flows are usually encountered in low-density flows where measurements on onset conditions are extremely difficult owing to very tiny droplets at onset and the heat addition zones show the structure of a weak compression wave. However, if the initial conditions are such that the left-running characteristics emanating from point O intersect, then the flow will be supercritical and shock waves arising from excessive heat addition and embedded in the rarefaction wave appear. In this case the left-running characteristics will approach each other forming the shock front KL of figure 5 where the origin K of the embedded shock front can be obtained by their envelope construction (this envelope construction resembles that in shock formation by compression waves resulting from a continuous acceleration of a piston initially at rest. In the latter case given the smooth piston path the construction of the envelope, thus the determination of the origin K of the

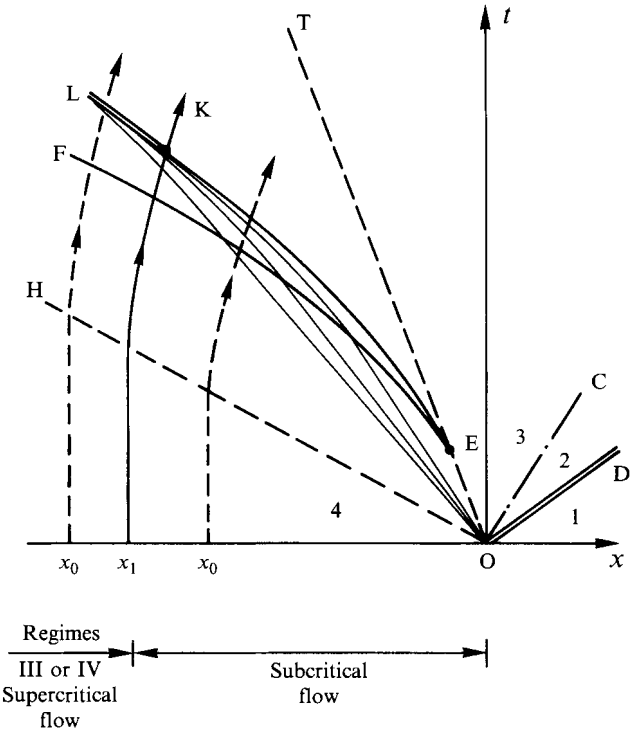

FIGURE 5. Global solution of supercritical flows with a weak embedded shock wave falling in either of the regimes III or IV of figure 4: EF is the condensation wave front, EK is the rarefaction wave tail and KL denotes the embedded shock front.

embedded shock, is possible analytically since the compression waves in this case are simple waves possessing Riemann invariants). The rarefaction wave tail EK, which is tangent to the envelope of the family of intersecting characteristics at K and to the frozen rarefaction tail OT at E, is formed by compressive effects due to heat addition when the initial frozen rarefaction tail OE (the portion ET of the frozen rarefaction wave OT in this case is virtual) enters the heat addition zones. Unfortunately identifying the origin K of the embedded shock wave, which marks the end of the rarefaction wave tail, is not analytically possible in this case since the equations for the left-running characteristics in the heat addition zones are not explicitly known.

Depending on the initial conditions point K may occur close to or far from point E (strong or weak embedded shock waves). If the initial conditions are such that the amount of heat added to the flow is sufficient for point K to lie far away (compared to flow length) from E, then the shock wave will be embedded in the heat addition zones of pathlines corresponding to supercritical flow regimes III or IV (weak embedded shock waves) as shown in figure 5. In this case the condensation wave front EF given by the condition $(\mathrm{d}B/\mathrm{d}t)_{t=t_l} = 0$ is located below the embedded shock wave for all pathlines initially at $x_0 < x_1$ where x_1 denotes the initial position of the pathline passing through point K. Thus on pathlines initially at x_0 where $x_1 < x_0 < 0$ the flow remains subcritical whereas on pathlines initially at x_0 where $x_0 < x_1$ the flow is supercritical falling in either of the regimes III or IV as shown in figure 5. When the initial conditions are such that more and more heat is added to the flow in the heat addition zones, the shock strength increases as we move away from point K along the shock front. In such a case the condensation wave front EF may intersect the

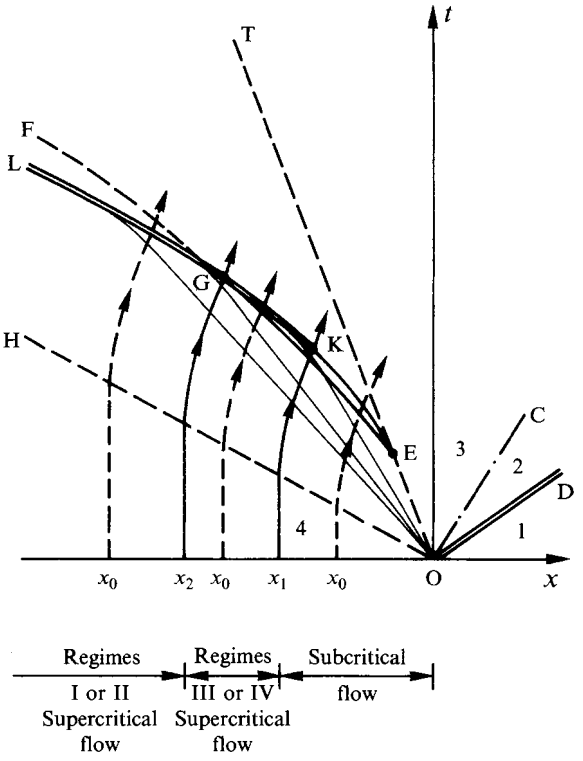

FIGURE 6. Global solution of supercritical flows with strong shock waves: EK is the rarefaction wave tail, KL is the embedded shock front and EF is the subcritical condensation wave front. The portion GF of EF is hypothetical and does not correspond to the onset conditions in this case.

embedded shock wave, say at point G (figure 6). Now if the pathlines passing through K and G have initial positions denoted by x_1 and x_2 respectively, the flow is subcritical on those pathlines initially at x_0 where $x_1 < x_0 < 0$, it is supercritical in either of the regimes III or IV for those pathlines initially at x_0 where $x_2 < x_0 < x_1$, and it is supercritical in either of the regimes I or II for those pathlines initially at x_0 where $x_0 < x_2$ as shown in figure 6. In this case the relative onset conditions, defined by the maximum available nucleation rate, for the pathlines which exhibit supercritical flow in either of the regimes I or II are no longer given by the front GF where $dB/dt = 0$, but by the shock front GL (the true onset conditions measured empirically lie in the onset zone of each regime as shown in figure 4*a–d*). The onset zones in front of the embedded shock now act as weak compression zones where the straight line characteristics (simple waves) emanating from point O are slightly curved due to heat addition. If the amount of heat released in the heat addition zones is increased any further, point G moves towards point K both approaching point E exhibiting strong shock behaviour.

To substantiate the above qualitative description of condensing shock tube flows with embedded shock waves, we return to the formidable problem of the computation of such flows. The computation in this case is fairly simple if the shock front KL can be constructed (shock fitting). In such a case the computation of the flow field along any pathline up to the shock front follows the same procedure as that for subcritical flows discussed in detail in §3 except in the onset zones where compression effects due to heat addition are felt more strongly than for subcritical flows resulting in the small

curvature of the left-running characteristics just upstream of the shock front. The flow variables just behind the shock along each pathline are then obtained by solving the shock relations (73)–(77). The computation of the flow field downstream of the shock along each pathline follows the same procedure as that in the heat addition zones of subcritical flows, namely by combining the asymptotic expressions for g and $\chi \equiv \mathrm{d}g/\mathrm{d}t$ in the heat addition zones downstream of the shock in each regime with the characteristic equations (29)–(32) and solving numerically by following a procedure similar to that for subcritical flows (semi-analytical solution). Unfortunately we are not in a position to introduce a shock fitting technique for these embedded shocks at this stage (the precise shock fitting technique introduced for embedded normal shock waves in condensing nozzle flows by the present authors (Delale *et al.* 1993*b*), based on the physical argument of accelerating the flow back to supersonic speeds by passing through a saddle point in the relaxation zones, does not apply in this case). Thus the shock fitting problem still remains open. In principle the shock may be fitted by trial and error starting at a chosen origin K; however, this seems impractical owing to the enormous amount of computation time required for a satisfactory solution. Nevertheless the qualitative global solution discussed above is very useful in interpreting the results of the experiments. The quantitative solution with embedded shocks will also be possible whenever a reliable shock fitting technique for such shocks is introduced on physical grounds (shock capturing methods as discussed by Roe 1986 and Moretti 1987 smear the embedded shock and are not useful here).

5. Asymptotic predictions of wave fronts and comparison with experiments

The asymptotic solution discussed above in §§3 and 4 respectively for subcritical and supercritical condensing shock tube flows can be computed (except for shock fitting) and compared with experiments by assuming a nucleation rate equation in the form of (24) and a droplet growth law in the form of (27) for a chosen condensable vapour. We would herein like to compare the asymptotic solution for the expansion of water vapour with different carrier gases (argon, nitrogen and air) for which experimental data are available (e.g. see Barschdorff 1975; Kalra 1975; Peters 1987). For the range of initial driver section temperatures investigated (T_4' typically between 295 and 300 K) the good agreement achieved in comparing the asymptotic solution of condensing nozzle flows by Delale *et al.* (1993*a*, *b*) with experiments by employing the classical nucleation theory and the Hertz–Knudsen droplet growth law together with some poorly known thermodynamic functions such as surface tension and condensation coefficient fitted to experiments, inspires us to use the same theories for nucleation and droplet growth law as a first comparison. For this reason we cast the classical nucleation rate equation into the normalized form of (24) (details are given in Delale *et al.* 1993*a*) with

$$\zeta' = \left(\frac{1}{500\pi}\right)^{1/2}\left(\frac{T_4'}{100}\right)^2 (m')^{-3/2}\frac{\omega_4^2\rho_4'^2}{\bar{\rho}_{con}}, \tag{78}$$

$$\Sigma(p,T,g) = \left(\frac{f(T)}{T^3}\right)^{1/2}\left(\frac{1-g/\omega_4}{1-g\mu_m/\mu_v}\right)^2 p^2, \tag{79}$$

$$B(p,T,g) = [f(T)]^3\,[\ln S(p,T,g)]^{-2}, \tag{80}$$

$$K = \frac{3\times 10^{15}}{16\pi}k^3\left(\frac{\bar{\rho}_{con}}{m'}\right)^2\left(\frac{100}{T_4'}\right)^9, \tag{81}$$

where the normalized surface tension $f(T)$ and supersaturation $S(p, T, g)$ are given by

$$f(T) = \begin{cases} (100/T_4')^4 [76.1 + 0.155(273.15 - T_4' T)]/T & \text{for} \quad T \geqslant 249.4K/T_4' \\ (11.31 - 0.03709 T_4' T)\, T^3 & \text{for} \quad T < 249.4K/T_4' \end{cases} \tag{82}$$

and

$$S(p, T, g) = \frac{p_4'}{T_4'^{C_1}} \frac{\mu_m(\omega_4 - g)}{(\mu_v - \mu_m g)} \frac{p}{T^{C_1} \exp[\nu_0 + \nu_1 T + \nu_2 T^2 + \nu_3/T]}, \tag{83}$$

with $\nu_0 = 21.125$, $\nu_1 = -2.7246 \times 10^{-2} T_4'$, $\nu_2 = 1.6853 \times 10^{-5} T_4'^2$, $\nu_3 = -6.095 \times 10^3 / T_4'$ and $C_1 = 2.4576$. In (78)–(83) m' is the mass of a single vapour molecule, $k = 1.38 \times 10^{-23}$ J K^{-1} is Boltzmann's constant, and it is implicit that the expression for the surface tension is obtained from a fit to the experiments of Peters & Paikert (1989) and that for the latent heat is obtained from Sonntag & Heinze (1982).

The Hertz–Knudsen droplet growth law can also be cast into the normalized form of (27) by following a procedure similar to that given in Delale *et al.* (1993*a*) with

$$\lambda = \frac{\Theta'}{r_d'} \left(\frac{T_4'}{100} \right)^{(C_1 - 0.5)} \frac{1}{\bar{\rho}_{con} (2\pi \Re / \mu_v)^{1/2}} \tag{84}$$

and

$$\Omega(p, T, g) = \alpha(T)\, 10^{2(C_1 - 0.5)} T^{(C_1 - 0.5)} \exp\left[\nu_0 + \nu_1 T + \nu_2 T^2 + \frac{\nu_3}{T} \right] \{S(p, T, g) - 1\}, \tag{85}$$

where the condensation coefficient $\alpha(T)$ is obtained from a fit to the experiments of Peters & Paikert (1989) and is given by

$$\alpha(T) = \begin{cases} 0.5 & \text{for} \quad T > 270K/T_4' \\ 1 - 0.0125(T_4' T - 230) & \text{for} \quad 230K/T_4' \leqslant T \leqslant 270K/T_4' \\ 1 & \text{for} \quad T < 230K/T_4'. \end{cases} \tag{86}$$

The normalized critical radius $r^*(p, T, g)$ can be conveniently obtained from the normalized Thomson–Gibbs equation as

$$r^*(p, T, g) = \frac{2m'}{10^5 r_d' \bar{\rho}_{con} k} \left(\frac{T_4'}{100} \right)^3 \frac{f(T)}{\ln S(p, T, g)}. \tag{87}$$

It is worth mentioning that all of the actual flow variables appearing in (78)–(87) are to be inserted in SI units. Equations (78)–(87) identify the parameters K and λ given respectively by (81) and (84) and the thermodynamic functions $\Sigma(p, T, g)$, $B(p, T, g)$, $\Omega(p, T, g)$ and $r^*(p, T, g)$ given respectively by (79), (80), (85) and (87) which enter the asymptotic expressions for the condensation rate equation.

Using the above information for identifying the thermodynamic functions and parameters that enter the asymptotic theory, an algorithm for the subcritical expansion of water vapour with a carrier gas is developed following the procedure described in detail in §3. By this algorithm the condensation wave front (EF in figure 1) is located precisely and the effect of heat addition on the flow field is exhibited semi-analytically (or semi-numerically) in the heat addition zones. The development of a similar algorithm for supercritical flows following the global solution of §4 unfortunately requires a shock fitting technique which is not readily available. Therefore, we restrict our computations only to subcritical or smooth flows. In fact for any working vapour and given initial driver and channel conditions, one must start with the solution of

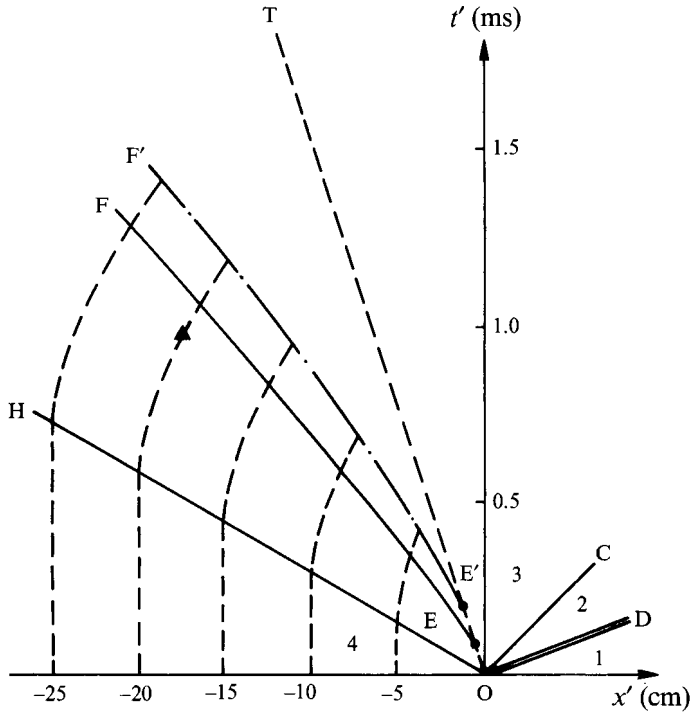

FIGURE 7. Condensation wave fronts for the expansion of water vapour in nitrogen in the rarefaction wave of a shock tube with initial driver section mixture pressure $p_4' = 680$ Torr, mixture temperature $T_4' = 295.3$ K, water vapour pressure $(p_v')_4 = 18.6$ Torr and initial channel air pressure $p_1' = 100$ Torr and air temperature $T_1' = 295.3$ K. E′F′ is the subcritical condensation wave front computed by Sislian & Glass (1976) by the method of characteristics, EF is the subcritical condensation wave front computed by the present asymptotic method and the symbol ▲ shows the experimental onset point of Kalra (1975).

subcritical flows to see whether or not the left-running characteristics intersect in the heat addition zones over lengths of practical importance. When the characteristics intersect (supercritical flow), embedded shock waves exist and the comparison with experimental data at this stage can only be made qualitatively from the results of §4.

To be able to compare the predictions of the asymptotic theory, at least for subcritical flows using the algorithm developed above for the expansion of water vapour with a carrier gas in the rarefaction wave, with the results of experiments and existing numerical computations, we first divide the experiments performed into two categories:

(*a*) experiments performed to predict the onset of condensation or the condensation wave front, and

(*b*) experiments dealing with the complete global solution with or without embedded shock waves in the rarefaction wave.

Various experiments falling in category (*a*) has been performed (e.g. Barschdorff 1975; Lee 1977; and Peters 1987). Among experiments falling into category (*b*) we can cite that by Kalra (1975) (also discussed in detail in Glass, Kalra & Sislian 1977) for the expansion of water vapour in nitrogen which is accompanied by the numerical computations of Sislian (1975). We herein choose to compare the predictions of the present asymptotic theory with these experiments. Figure 7 shows the predictions of the asymptotic theory in the wave diagram using the above subcritical algorithm for

the experiments of Kalra (1975). The curves EF and E′F′ are respectively the condensation wave fronts predicted by the present asymptotic theory and by the numerical computations of Sislian & Glass (1976) which presents a brief summary of the results of the numerical computations of Sislian (1975) (it is important to mention that the observable difference between the two condensation fronts in figure 7 is not due to the method of prediction, but it arises mainly because different expressions for the surface tension and for the condensation coefficient are employed). As can clearly be seen from the figure, although the employment of the normalized surface tension $f(T)$ given by (82) and of the condensation coefficient $\alpha(T)$ given by (86) in the classical nucleation theory and Hertz–Knudsen droplet growth law seems to have improved the prediction for the condensation wave front by Sislian & Glass (1976), the difference between the experimental onset point of Kalra (1975) at the observation station and the present prediction is still appreciable. Despite the fact that the thermodynamic properties employed herein for the vapour phase for a similar change of state have proved to provide good agreement of the asymptotic predictions with the results of condensing nozzle experiments (see Delale *et al.* 1993*a*, *b*), this difference in the onset conditions between the above prediction and experiments should be expected. The reason is that the experiments of Kalra (1975) show embedded shock waves due to excessive heat addition, which presumably fall in either of the regimes I or II along the pathline passing through the experimental onset point at the observation station. Now from the qualitative results of §4 (see figure 6), it seems that the embedded shock lies below the condensation wave front EF at the observation station, which is precisely the case here as shown in the x–t diagram of figure 7. Thus the curve EF in this case should not be called the condensation wave front, but should be interpreted as the maximum accessible nucleation or supersaturation front if the flow were continued downstream along those pathlines meeting the shock front in a smooth or subcritical manner. In fact when we continue our subcritical calculation for the conditions stated in figure 7 beyond the curve EF in the heat addition zones, we immediately encounter very large gradients (e.g. on a typical pathline initially at $x_0' = -5$ cm, $\mathrm{d}p'/\mathrm{d}t'$ is of the order of 10^{12} Pa s^{-1}) resulting in the intersections of the left-running characteristics which obviously support the above interpretation (the numerical computations of Sislian & Glass 1976 also show intersecting characteristics of the same family in the heat addition zones supporting the above interpretation).

We now proceed to compare the predictions of the asymptotic theory with experiments of category (*a*) aimed to predict solely the onset of condensation. Unfortunately, for these experiments there is no evidence whether the flow is subcritical or supercritical. Thus we have to rely upon our computations in the heat addition zones. Figure 8 shows the subcritical asymptotic predictions for the onset of condensation for the expansion of water vapour in argon in the experiments of Barschdorff (1975) and Peters (1987). The differences between the present predictions and the experimental onset conditions of Barschdorff suggest that the flow is most probably supercritical, falling in one of the regimes I or II (supported by intersecting characteristics in the heat addition zones). The better agreement of the predicted onset conditions at low pressures with Peters' experiments is not surprising since in this case, because of sufficiently low density, the flow is either subcritical or supercritical with a weak embedded shock wave falling either in regime III or IV (to our regret we are not able to decide whether the flow at the observation station is subcritical or supercritical since the initial channel conditions in Peters' experiments are not specified). Finally figure 9 shows the onset conditions in the experiments of Barschdorff (1975) for the expansion of moist air. The differences between the predicted conditions and the

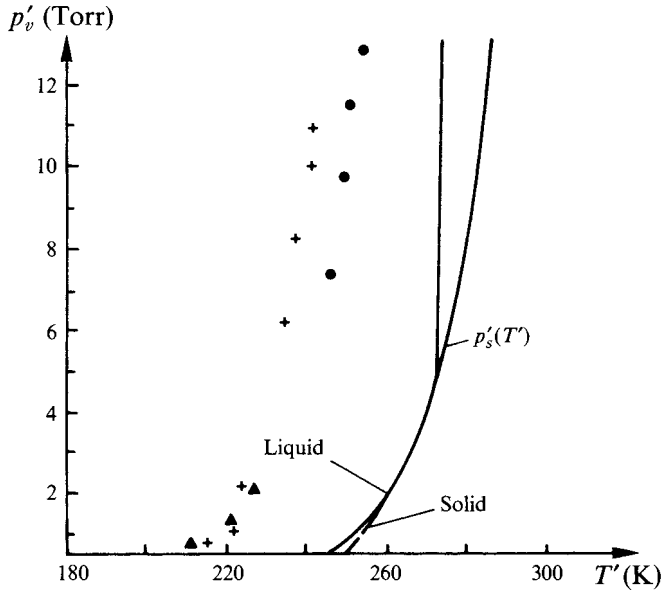

FIGURE 8. The onset conditions for the expansion of water vapour in argon in a shock tube where $p'_s(T')$ denotes the saturation pressure: ●, the experimental data of Barschdorff (1975); ▲, the experimental data of Peters (1987); +, the present asymptotic predictions assuming subcritical flow.

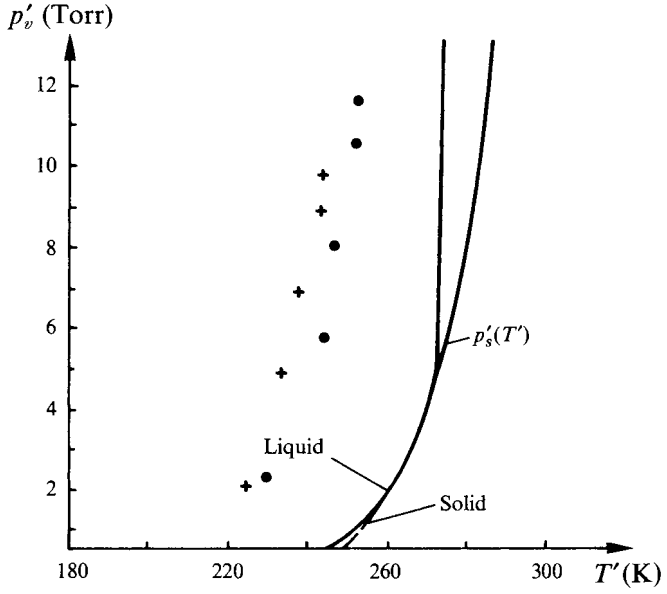

FIGURE 9. The onset conditions for the expansion of moist air in a shock tube where $p'_s(T')$ denotes the saturation pressure: ●, the experimental data of Barschdorff (1975); +, the present asymptotic predictions assuming subcritical flow.

experimental results at the observation station can also be interpreted on the basis of whether the flow therein is supercritical or subcritical in a manner similar to that done for figure 8. Once again the differences between the predicted results and the experiments seem to vanish as the initial partial vapour pressures are lowered, approaching the conditions for subcritical flows.

The differences in figures 7–9 between experiments and asymptotic predictions for the onset conditions of water vapour in various experiments are interpreted as to have arisen mainly from the existence of embedded shock waves falling in either of the regimes I or II. Unfortunately, a simple shock fitting technique to fit the embedded shock wave is not available yet, so we do not really know how much of the differences will be removed. Even when the computations with embedded shocks are successfully carried out, some of these differences for the onset conditions may still prevail. These remaining differences may arise from:

(i) the neglect of the heterogeneous nucleation mechanism;

(ii) the use of the classical nucleation theory and Hertz–Knudsen droplet growth law together with the choice of certain poorly known thermodynamic properties such as surface tension and accommodation coefficients;

(iii) the use of planar centred expansion wave theory;

(iv) the neglect of other non-equilibrium relaxation modes such as the relaxation of the velocity slip and droplet temperature in the case of a two-velocity and two-temperature model of the two-phase mixture;

(v) the neglect of viscous, heat conduction and diffusive effects;

(vi) the neglect of unsteady effects that may arise from condensation dynamics, and

(vii) the level of precision achieved in determining the experimental onset conditions.

Some of these effects have already been taken into account in various studies (e.g. Kotake & Glass 1977 consider the effect of heterogeneous nucleation, Lee 1977 and Glass *et al.* 1977 take into account the shift of the origin of the rarefaction wave); however, the differences between experiments and predictions do not diminish satisfactorily. This fact also supports the view that what is mainly responsible for the differences in the onset conditions between experiment and theory is neglecting or smoothing out embedded shock waves, as has been discussed in detail in this investigation.

6. Discussion

The asymptotic solution for shock tube flows with homogeneous condensation (the Riemann problem with homogeneous condensation) is presented for both smooth (subcritical) flows and flows with embedded shock waves arising from excessive heat release by condensation (supercritical flows). The global solution for subcritical flows where the flow is smooth along any chosen pathline is described both qualitatively and quantitatively (the solution in this case is completely analytical up to the onset of condensation and semi-analytical in the heat addition zones). For supercritical flows four distinct flow regimes, which may occur along any pathline intersecting the shock front, are distinguished from the asymptotic solution of the rate equation with embedded shocks. The global solution for supercritical flows is only qualitatively discussed owing to lack of a shock fitting technique for embedded shock waves. A subcritical flow algorithm for the expansion of water vapour in a carrier gas, which locates the condensation wave front precisely (analytically) is developed and applied to various experiments. With the results of the qualitative global solution of supercritical flows, the causes of the differences between the subcritical asymptotic predictions and the experimental onset conditions at the observation station are discussed and identified.

It is shown that most of the experiments performed to date to predict the onset of condensation show supercritical behaviour with intersecting left-running characteristics in the heat addition zones. Differences between the experimental onset

conditions and the predicted subcritical condensation wave front (which has been incorrectly interpreted as onset of condensation for these experiments) then naturally arise since nucleation rates are quenched by the embedded shock along pathlines before reaching their maximum accessible values at the subcritical condensation wave front. Aside from these major differences, other differences which arise from possible sources discussed at the end of §5 may also occur.

This work clarifies some of the most important features of shock tube flows with homogeneous condensation, especially by elucidating the nature of the differences between the experimental onset conditions and the predicted condensation wave fronts. It remains to introduce a shock fitting technique for embedded shock waves which will render the qualitative global solution of supercritical flows discussed in §4 quantitative and which will make the computations of such flows possible. This is the main objective to be achieved in the future.

The authors are grateful to Professor Dr B. Schmidt for useful discussions. One of us (C.F.D) acknowledges the support by the Alexander von Humboldt Foundation without which this work would have been impossible.

REFERENCES

ABRAMOWITZ, M. & STEGUN, A. 1965 *Handbook of Mathematical Functions*. Dover.

BARSCHDORFF, D. 1975 Carrier gas effects on homogeneous nucleation of water vapor in a shock tube. *Phys. Fluids* **18**, 529–535.

BLYTHE, P. A. & SHIH, C. J. 1976 Condensation shocks in nozzle flows. *J. Fluid Mech.* **76**, 593–621.

CLARKE, J. H. & DELALE, C. F. 1986 Nozzle flows with nonequilibrium condensation. *Phys. Fluids* **29**, 1398–1413.

COURTNEY, W. G. 1965 Condensation in a rarefaction wave. *Tech. Rep.* 2 ONR NR 092 517/4-29-65. Tiokol Chemical Corp., Denville, New Jersey.

DELALE, C. F., SCHNERR, G. H. & ZIEREP, J. 1993*a* Asymptotic solution of transonic nozzle flows with homogeneous condensation. I. Subcritical flows. *Phys. Fluids* A **5**, 2969–2981.

DELALE, C. F., SCHNERR, G. H. & ZIEREP, J. 1993*b* Asymptotic solution of transonic nozzle flows with homogeneous condensation. II. Supercritical flows. *Phys. Fluids* A **5**, 2982–2995.

ERDELYI, A. 1956 *Asymptotic Expansions*. Dover.

GLASS, I. I., KALRA, S. P. & SISLIAN, J. P. 1977 Condensation of water vapor in rarefaction waves. III. Experimental results. *AIAA J.* **15**, 686–693.

GLASS, I. I. & PATTERSON, G. N. 1955 A theoretical and experimental study of shock tube flows. *J. Aero. Sci.* **22**, 75–100.

GRADSHTEYN, I. S. & RYZHIK, I. M. 1980 *Tables of Integrals, Series and Products*. Academic.

HOMER, J. B. 1971 Studies on nucleation and growth of metallic particles from supersaturated vapors. *Shock Tube Research, Proc. Eighth Intl Shock Tube Symp., London* (ed. J. L. Stollery, A. G. Gaydon & P. R. Owen). Chapman and Hall.

KALRA, S. P. 1975 Experiments on nonequilibrium, nonstationary expansion of water vapor/carrier gas mixture in a shock tube. *University of Toronto, Institute for Aerospace Studies, Rep.* 195.

KAWADA, H. & MORI, Y. 1973 A shock tube study on condensation kinetics. *Bull. JSME* **16**, 1053–1066.

KOTAKE, S. & GLASS, I. I. 1977 Condensation of water vapor in rarefaction waves. II. Heterogeneous nucleation. *AIAA J.* **15**, 215–221.

LAX, P. D. 1954 Weak solutions of nonlinear hyperbolic equations and their numerical computation. *Commun. Pure Appl. Maths* **7**, 159–193.

LEE, C. F. 1977 Condensation of H_2O and D_2O in argon in the centred expansion wave in a shock tube. *ASME Symp. on Condensation in High Speed Flows* (ed. A. A. Pouring), pp. 83–96. US Naval Academy.

MORETTI, G. 1987 Computation of flows with shocks. *Ann. Rev. Fluid Mech.* **19**, 313–337.

PETERS, F. 1987 Condensation of supersaturated water vapor at low temperatures in a shock tube. *J. Phys. Chem.* **91**, 2487–2489.

PETERS, F. & PAIKERT, B. 1989 Nucleation and growth rates of homogeneously condensing water vapor in argon from shock tube experiments. *Exps. Fluids* **7**, 521–530.

ROE, P. L. 1986 Characteristic based schemes for the Euler equations. *Ann. Rev. Fluid Mech.* **18**, 337–365.

SIROVICH, L. 1971 *Techniques of Asymptotic Analysis.* Springer.

SISLIAN, J. P. 1975 Condensation of water vapor with or without a carrier gas in a shock tube. *University of Toronto, Institute for Aerospace Studies, Rep.* 201.

SISLIAN, J. P. & GLASS, I. I. 1976 Condensation of water vapor in rarefaction waves. I. Homogeneous nucleation. *AIAA J.* **14**, 1731–1737.

SMOLDERS, H. J. 1992 Nonlinear wave phenomena in a gas-vapour-droplets mixture with phase transition. *Proefschrift.* Eindhoven University of Technology.

SMOLDERS, H. J., NIESSEN, E. M. J. & DONGEN, M. E. H. VAN 1992 The random choice method applied to nonlinear wave propagation in gas-vapour-droplets mixtures. *Computers Fluids* **21**, 63–75.

SONNTAG, D. & HEINZE, D. 1982 *Sättigungsdampfdruck- und Sättigungsdampfdichtetafeln für Wasser und Eis.* Leipzig: VEB Deutscher-Verlag.

VINCENTI, G. W. & KRUGER, C. H. 1965 *Introduction to Physical Gas Dynamics.* Wiley.

WEGENER, P. P. & LUNDQUIST, G. 1951 Condensation of water vapor in a shock tube below 150° K. *J. Appl. Phys.* **22**, 233.

WHITHAM, G. B. 1974 *Linear and Nonlinear Waves.* Wiley.

WU, B. J. C. 1977 Analysis of condensation in the centred expansion wave in a shock tube. *ASME Symp. on Condensation in High Speed Flows* (ed. A. A. Pouring), pp. 73–82. US Naval Academy.

ZETTLEMOYER, A. C. 1969 *Nucleation.* Marcel Dekker.